FACTA UNIVERSITATIS (NIŠ)
SER.: ELEC. ENERG. vol. 15, No. 2, Aug. 2002, 205-216

A Fast Forward Solution with a Boundary Element Method for Eddy Current Nondestructive Testing

Hermann F. Uhlmann and Olaf Michelsson

Abstract: Eddy current non-destructive testing is used to determine position and size of cracks or other defects in conducting materials. The presence of a crack normal to the excited eddy currents distorts the magnetic field; so for the identification of defects a very accurate and fast 3D-computation of the magnetic field is necessary. A computation scheme for 3D quasistatic electromagnetic fields by means of the Boundary Element Method is presented. Although the use of constant field approximations on boundary elements is the easiest way, it often provides an insufficient accuracy. This can be overcome by higher order approximation schemes.

The numerical results are compared against some analytically solvable arrangements.

Keywords: Boundary element method, eddy currents, non-destructive testing.

1 Introduction

Boundary Element Methods (BEM) are widely used for the numerical solution of partially differential equations, e. g. in electromagnetics or structure mechanics. Its advantages - reduction to a discretized surface, implicit handling of unbounded regions - can be applied excellently to many purposes. On the other hand there are disadvantages. A BEM can only be applied to linear materials, the resulting system matrix is dense and often

Manuscript received May 14, 2002. A version of this paper was presented at the Fifth International Conference on Applied Electromagnetics, ПЕS 2001, October 8 -10, 2001, Niš, Serbia.

The autors are with Technische Universität Ilmenau, P.O.Box 100565, D-98684 Ilmenau, Germany, e-mails: [Hermann.Uhlmann, Olaf.Michelsonn]@TU-Ilmenau.de).

ill conditioned. Especially the large matrices are limiting factors for three-dimensional computations.

For complicated geometries, where a high precision of the solution is demanded, typically used linear triangles with constant field approaches on them cannot fulfil the requirements without tremendous memory amounts. As a consequence, approaches based on higher-degree polynomials will be considered.

In order to decrease the number of unknowns, usually the field values on corners or edges of the boundary elements, respectively, are expanded using higher degree polynomial shape functions. This leads to a higher approximation quality and reduces at the same time the number of unknowns. However, it causes problems in the integration of terms with singularities, which occur in integral formulations. Another difficulty arises due to a not uniquely defined normal vector on corners/edges.

We discuss solutions to these problems. Higher-degree polynomial approaches are introduced for the calculation of eddy currents.

2 The Field Calculation with BEM

The used integral formulation is the so-called $\boldsymbol{H}$-φ-method, proposed by Mayergoyz [1] and firstly implemented with constant triangular elements by Lavers and Kalaichelvan [2,3]. This method, which uses two separate imaginary sources, is of minimum order.

2.1 The H-φ-formulation

A homogeneous conducting region Ω^+ with constant conductivity κ and permeability μ is considered.

The surrounding air region Ω^- includes the source field $\boldsymbol{H}_S^-$, with the angular frequency ω, included by the exciting current $\boldsymbol{I}_S^-$.

Inside the conducting region the magnetic field $\boldsymbol{H}^+$ can be described by a virtual current density $\tilde{\boldsymbol{J}}$ on the interface Γ between Ω^+ and Ω^-

$$\boldsymbol{H}^+(r) = \int \nabla_r \times \left[\tilde{\boldsymbol{J}}(r')G(\boldsymbol{r},\boldsymbol{r}')\right] \mathrm{d}\Gamma \tag{1}$$

with Green's function,

$$G(\boldsymbol{r},\boldsymbol{r}') = \frac{1}{4\pi R} e^{-j\beta R}, \quad R = |\boldsymbol{r} - \boldsymbol{r}'|,$$

where $\boldsymbol{r}$ and $\boldsymbol{r}'$ denote the field point and source point, respectively.

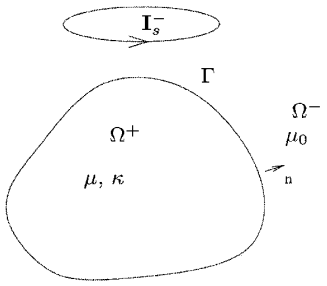

Fig. 1. A conductor exposed to an exciting electromagnetic field.

The magnetic field $\boldsymbol{H}^-$ in the non-conducting region Ω^- is given as the sum of the imposed field and the irrotational scattered field from the conducting material. It can be represented by a magnetic scalar potential φ_m, which in turn is described by the surface charge density σ_m:

$$H^-(r) = H_s^-(r) - \nabla\varphi_m(r) \tag{2}$$

$$\varphi_{\mathrm{m}}(\boldsymbol{r}) = \int \sigma_m(\boldsymbol{r}')G^a(\boldsymbol{r},\boldsymbol{r}')\mathrm{d}\Gamma, \tag{3}$$

where

$$\mathrm{G}^a(\boldsymbol{r},\boldsymbol{r}') = \frac{1}{4\pi R}$$

is the free-space Green's function and Γ denotes the interface.

If equations (1) and (2) satisfy the interface conditions, a boundary integral equations system can be set up. The equations can be noted as follows [4]

$$\begin{aligned}\frac{\Omega_S}{4\pi}\tilde{\boldsymbol{J}}(\boldsymbol{r}) + \int_\Gamma \boldsymbol{n_r} \times \Big[\tilde{\boldsymbol{J}}(\boldsymbol{r}') \times \nabla_r G\Big]\mathrm{d}\Gamma_{r'} \\ - \int_\Gamma \sigma_m(\boldsymbol{r}')\Big[\boldsymbol{n_r} \times \nabla_r G^a\Big]\mathrm{d}\Gamma_{r'} = -\boldsymbol{n_r} \times \boldsymbol{H}_S^-(\boldsymbol{r}),\end{aligned} \tag{4}$$

$$\begin{aligned}\frac{\Omega_S}{4\pi}\sigma_m(\boldsymbol{r}) - \int_\Gamma \sigma_m(\boldsymbol{r}')\Big[\boldsymbol{n_r}\nabla_r G^a\Big]\mathrm{d}\Gamma_{r'} \\ + \frac{\mu}{\mu_0}\int_\Gamma \boldsymbol{n_r}\Big[\tilde{\boldsymbol{J}}(\boldsymbol{r}') \times \nabla_r G\Big]\mathrm{d}\Gamma = -\boldsymbol{n_r}\boldsymbol{H}_S^-(\boldsymbol{r}),\end{aligned} \tag{5}$$

where Ω_S is the solid angle of the field point.

Since for the above integral equations exists no closed solution in general, the solution domain is splitted into discrete simply shaped surfaces elements. On these so-called Boundary Elements (BE) the surface values can be approximated using shape functions,

$$F(\xi,\eta) = \sum_{k=1}^{n} N_k(\xi,\eta) F_k,$$

where ξ and η are local coordinates in the BE. The shape-functions $N_k(\xi,\eta)$ are two-dimensional polynomials, defined on standard-elements [5]. They allow an easy and consistent handling of the field values and their derivatives as well as the description of the boundary element geometry.

According to the weighted residual method the surface integral equation will then be multiplied by a local test-function, which defines the way the approximated solution fits the exact solution. The most commonly used variants are point collocation and Galerkin's method.

In our application we used simply the point-collocation, because this implies only a point-to-element integration, whereas the Galerkin's approach needs an element-to-element integration, which is much more complicated and time-expensive. A combination of both methods is described in [6].

The simplest approximation is a constant field value on each single BE. This approximation scheme has advantages not only in its simple integration, it also provides a discontinuity between adjacent elements, which makes it a good approximation strategy on corners/edges, where the field values are intrinsically discontinuous. However, its accuracy is not high, a fine discretization is required.

Better approximations can be achieved using linear or quadratic shape functions. Linear shape functions use at most the same number of unknowns as constant elements for the same discretization, but provide a far better accuracy. This is due to the fact, that C_0- continuity of surface values between adjacent BE is assumed. If this continuity is violated due to geometrical properties where the normal vector is discontinuous, special precautions are required.

As result of the discretization a linear equation system can be assembled:

$$M \begin{bmatrix} \tilde{\boldsymbol{J}} \\ \sigma_m \end{bmatrix} = \begin{bmatrix} -\boldsymbol{n} \times \boldsymbol{H}_S^- \\ -\boldsymbol{n}\boldsymbol{H}_S^- \end{bmatrix} \tag{6}$$

where M denotes the system matrix, which contains the integral interaction between all nodal surface values. A special notation for triangular elements using constant shape functions can be found in [7].

The magnetic field in all regions can be calculated using (1,2) from the solution of the virtual surface values in (6).

The electrical filed in Ω^+ can be calculated by

$$\mathbf{J} = \int_\Gamma \nabla \times \left[\nabla \times (\tilde{\mathbf{J}} \mathrm{G}) \right] \mathrm{d}\Gamma, \tag{7}$$

where $\boldsymbol{J}$ denotes the real eddy current density in the conducting region.

2.2 Treatment of Integrals

A main problem in the BEM is the exact calculation of the singular integrals. In the used formulation integrals of order $O(r^{-2})$ arise. They can only be calculated on the sense of a Cauchy principal value. For constant triangular elements an integration area can be found, where the integral around the singular point vanishes. But this simple method is not applicable for higher order shape functions. Therefore we implemented a Taylor expansion scheme proposed in [8], which yields excellent results. Also the calculation of nearly singular integrals can be done with this method combined with an adaptive subtriangulation scheme [9].

All other integrals can be performed efficiently using selected Gauss-integration schemes. The number of Gauss-points can be made dependent on the factor λ, which is defined as

$$\lambda = \frac{l_{max}}{R}, \tag{8}$$

where l_{max} is the largest distance in the integration area and R is the average distance between the field point and the integration area.

3 Crack Simulation

Eddy current testing is used to determine position and size of cracks or defects in conducting materials. The measured magnetic field is generated by the interaction between the testing specimen and an exciting coil.

The simulation of a crack can be done by a direct geometrical model or by secondary sources. The direct model has many disadvantages. It implies, that the impedance change in the exciting coil will be calculated as the difference of the impedance between the disturbed and the undisturbed case, but the impedance change cannot be calculated accurately.

A better numerical signal/noise ratio can be reached, if small material defects are modelled as secondary sources. Maxwell's equation for an

isotropic conductor containing a local conductivity variation may be written as

$$\nabla \times \boldsymbol{E}(\boldsymbol{r}) = -j\omega\mu_0 \boldsymbol{H}(\boldsymbol{r}), \tag{9}$$

$$\begin{aligned} \nabla \times \boldsymbol{H}(\boldsymbol{r}) &= \kappa(\boldsymbol{r})\boldsymbol{E}(\boldsymbol{r}) \\ &= \kappa_0 \boldsymbol{E}(\boldsymbol{r}) + [\kappa(\boldsymbol{r}) - \kappa_0]\boldsymbol{E}(\boldsymbol{r}). \end{aligned} \tag{10}$$

The last term in (10) can be interpreted as a secondary current dipole density $\boldsymbol{P}(\boldsymbol{r})$ at the flaw due to departures from an otherwise constant conductivity κ_0.

Then the electrical field in any point in a conducting free space can be expressed as

$$\boldsymbol{E}(\boldsymbol{r}) = \boldsymbol{E}^i(\boldsymbol{r}) - j\omega\mu_0 \int_{\text{flaw}} \bar{\boldsymbol{G}}_e^0(\boldsymbol{r}, \boldsymbol{r}')\boldsymbol{P}(\boldsymbol{r}')\mathrm{d}\boldsymbol{r}', \tag{11}$$

where $\boldsymbol{E}^i(\boldsymbol{r})$ is the incident or unperturbed field. The integral represents the electrical field scattered by the flaw. The operator $\bar{\boldsymbol{G}}_e^0(\boldsymbol{r}, \boldsymbol{r}')$ is the electrical-electrical Green's function for the free space in conducting materials, which is the solution of

$$\nabla \times \nabla \times \bar{\boldsymbol{G}}_e^0(\boldsymbol{r}, \boldsymbol{r}') + \beta^2 \bar{\boldsymbol{G}}_e^0(\boldsymbol{r}, \boldsymbol{r}') = \delta(\boldsymbol{r} - \boldsymbol{r}')\bar{\boldsymbol{I}}. \tag{12}$$

It can be expressed by

$$\bar{\boldsymbol{G}}_e^0(\boldsymbol{r}, \boldsymbol{r}') = \left[\bar{\boldsymbol{I}} - \frac{1}{\beta^2}\nabla\nabla\right]\boldsymbol{G}(\boldsymbol{r}, \boldsymbol{r}'), \tag{13}$$

where

$$\beta^2 = -j\omega\kappa\mu_0$$

and the unit dyadic

$$\bar{\boldsymbol{I}} = \hat{x}\hat{x} + \hat{y}\hat{y} + \hat{z}\hat{z}$$

are used.

The reflections due to the material boundaries are calculated using the presented BEM with a flaw function $v = (\kappa r - \kappa_0)\kappa_0$ and (7) this leads to

$$\boldsymbol{P}(\boldsymbol{r}) = \boldsymbol{P}^i(\boldsymbol{r}) + v(\boldsymbol{r})\beta^2 \int_{\text{flaw}} \bar{\boldsymbol{G}}_e^0(\boldsymbol{r}, \boldsymbol{r}')\boldsymbol{P}(\boldsymbol{r}')\mathrm{d}\boldsymbol{r}' - v(\boldsymbol{r})\boldsymbol{J}_{\text{BEM}}, \tag{14}$$

where

$$\boldsymbol{P}^i(\boldsymbol{r}) = \kappa_0 v(\boldsymbol{r})\boldsymbol{E}^i(\boldsymbol{r})$$

vanishes at points outside the flaw.

The dipole current density in the flaw is used as a source for the BEM field solution program. The right hand side of the equation system (6) can be calculated using the electrical-magnetic Green's function

$$H(r) = \int_{\text{flaw}} \bar{\boldsymbol{G}}_m^0(\boldsymbol{r}, \boldsymbol{r}')\boldsymbol{P}\mathrm{d}\boldsymbol{r}', \tag{15}$$

$$\bar{\mathbf{G}}_m^0(\boldsymbol{r}, \boldsymbol{r}') = \frac{1}{4\pi}\nabla \times (G(\boldsymbol{r}, \boldsymbol{r}')\bar{\boldsymbol{I}}). \tag{16}$$

Using the virtual current density $\tilde{J}$ the reacting current density $\boldsymbol{J}_{\text{BEM}}$ in the material can be calculated with (7).

All computations of the dependences between the sources, the right hand side, the virtually surface values and the real currents in the material are carried out by simple matrix multiplications. Therefore these calculations can be performed very fast.

For the computation of the dipole current density the flaw region can be splitted into small volume elements where the dipoles in the centre of each cell are expanded with constant shape functions over the cell volume, quite similar to a formulation given by [10].

The calculation of the integral in (14) concerning the Green's function $\bar{\boldsymbol{G}}_e^0(\boldsymbol{r}, \boldsymbol{r}')$ can be performed using a method proposed in [11]. This leads to a linear equation system

$$\boldsymbol{P}_i = \boldsymbol{P}_i^i + v_i\Big[\boldsymbol{A}_{\bar{\boldsymbol{G}}_e^0}\boldsymbol{P}_j + \boldsymbol{B}_{\text{BEM}}\boldsymbol{P}_j\Big] \tag{17}$$

which can be solved using a SOR iterative solver. The matrix $\boldsymbol{A}_{\bar{\boldsymbol{G}}_e^0}$ contains the integrals over $\bar{\boldsymbol{G}}_m^0(\boldsymbol{r}, \boldsymbol{r}')$ between each cell, matrix $\boldsymbol{B}_{\text{BEM}}$ contains the integral dependences built by the Boundary Element formulation.

The calculation of the impedance change in the exciting coil than can be done using the reciprocity in the form

$$I^2\Delta Z = -\int_{\text{flaw}} \boldsymbol{E}^i(\boldsymbol{r})\boldsymbol{P}(\boldsymbol{r})\mathrm{d}\boldsymbol{r}, \tag{18}$$

where ΔZ denotes the impedance change.

4 Numerical Results

A sensible arrangement is a solid sphere consisting of permeable conducting material. Because in this case elements outside the main-diagonal are scaled-up the system matrix becomes ill conditioned.

As an example in Fig. 2 the z-component of the magnetic field-strength along the z-axis is shown, where the relative permeability is now set to $\mu_r = 100$. The solution follows the discontinuity of the magnetic filed strength very close, which can be seen in the zoomed part. The relative error of the magnitude and the phase-difference to the analytical solution are shown in Fig. 3.

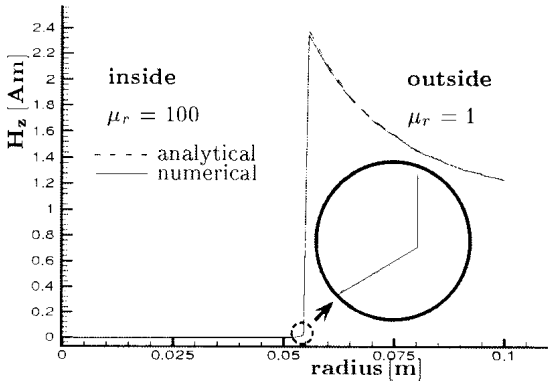

Fig. 2. Radial component of the magnetic field strength for a sphere with $\mu = 100$ in comparison to the analytical solution. The inset shows the field near the surface inside the sphere.

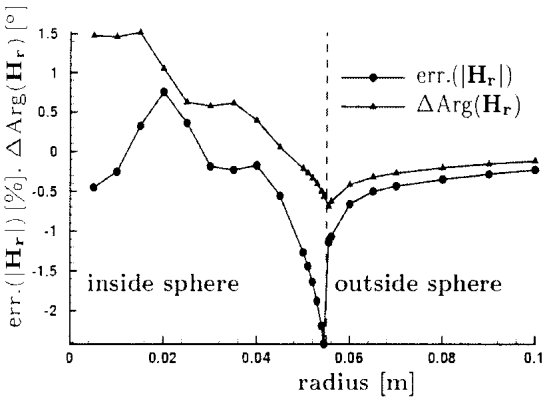

Fig. 3. Relative error of the radial component and the phase difference along the radius of the sphere with $\mu_r = 100$.

In order to compare the accuracy of the algorithm we calculated the impedance change of a coil according to the TEAM Benchmark Problem No. 15.

The calculations of the eddy current density in the flaw in the unperturbed case were performed with a large model of a finite plate as given in the benchmark setup, whereas the crack simulations were performed on a much smaller model assuming a half space. This assumption does not influence the accuracy significantly.

In the figures 4 and 5 the absolute value and argument of the variation of ΔZ are shown for different locations of the exciting coil along the slot from its centre.

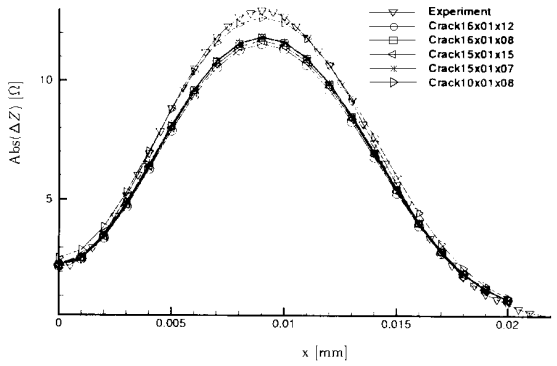

Fig. 4. Comparison of the absolute impedance variation of ΔZ for different crack discretization.

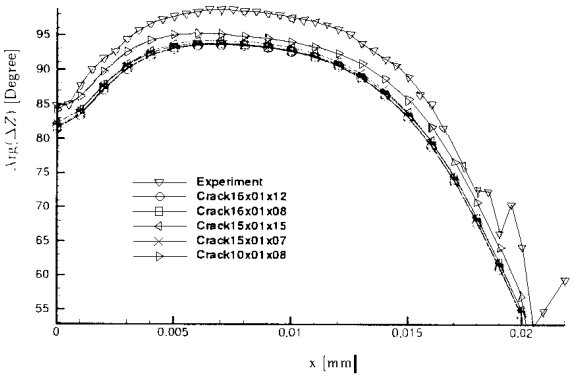

Fig. 5. Comparison of the phase of ΔZ for different crack discretization.

The results are in good agreement with this measured data.

It can be seen, that a refinement of the crack discretization does not improve the accuracy. This is due to the singular behaviour of the Bound-

ary Element formulation directly on the surface, where the crack volume is located very close to the surface of the conductor. The surface discretization influences the accuracy very strong in this region. Further improvements in the model should be focused on this problem.

Furthermore, the sixth TEAM benchmark problem [12], the conducting hollow sphere in an uniform magnetic field, has been solved successfully.

The magnetic induction for the hollow sphere along the x-axis is shown in Fig. 6. It can be seen, that the numerical solution is in very good agreement with the analytical one.

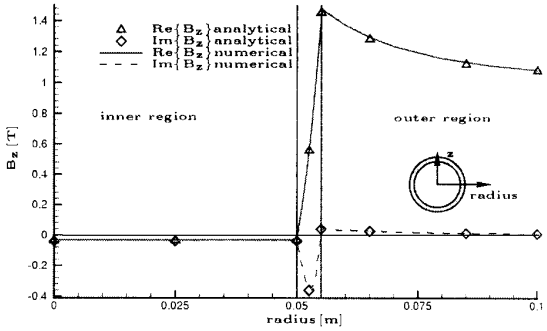

Fig. 6. The z-component of the magnetic induction along x-axis of the hollow sphere in TEAM benchmark problen No. 6.

In Table 1 a comparison between the constant and quadratically approximated field values for the calculation of the hollow sphere is shown. The advantages of the quadratic approximation are very convincing.

Table 1. Comparison Between Constant Quadratic Shape Functions for the computation of the sixth TEAM Benchmark Problem.

	Constant	Quadratic
Number of elements	960	144
Rel. error of magnitude	~10%	< 3%
Error of phase angle	< 5°	< 1°
Number of unknowns	2880	1168
Memory requirements	127 Mb	11 Mb
CPU-time (HP J282)	1800s	1140s

For the solution of the linear equation system various solvers have been tested. Direct solvers like LU-decomposition and back-substitution, lead always to a solution, but can suffer from numerical errors on large matrices. Iterative solvers can find a solution with much lower computational costs, but

their convergence depends strongly on the condition of the system matrix. Various tests were performed to check the stability of several iterative solvers. In Figure 7 the convergence speed is shown for some typically used iterative solvers.

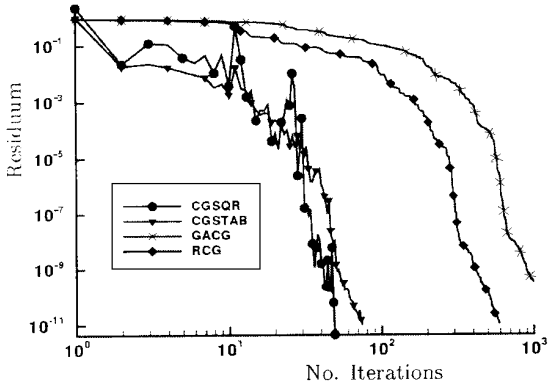

Fig. 7. Comparison of the convergence speed between various iterative solvers.

In summary a complex conjugate gradient-squared algorithm (CGS) gave the best results.

As performance is always an important question in numerical field computation, the use of hardware-optimised BLAS-libraries (Basic Linear Algebra Subroutines, at ftp.netlib.org) is strongly recommended. This speeds up the computation typically by a factor of two.

5 Conclusion

A Boundary Element Method for the calculation of quasi-static fields was presented. The use of higher order shape functions for the approximation of field values leads to highly accurate results. In combination with the advantages of Boundary Element Methods in general, the method is very useful for field calculations in unbounded regions.

Due to precise calculation of the strongly singular integrals combined with stable iterative solvers the implemented algorithm can also be used for accurate calculation of eddy currents in permeable materials.

The increased numerical expense for the treatment of higher order approximation functions yields on the other hand more accurate results and a decreased number of unknowns.

References

[1] I. Mayergoyz: *Boundary integral equations of minimum order for the calculation of three-dimensional eddy current problems*, IEEE Transactions on Magnetics, Vol. 18, no. 1, pp. 536-539, 1982.

[2] S. Kalaichelvan, J. Lavers: *Boundary Element Methods for Eddy Current Problems, vol. 6: Electromagnetic Applications of Topics in Boundary Element Research*, ch. 4, Springer Verlag, Berlin, 1989.

[3] S. Kalaichelvan: *A Boundary Integral Equation Method for 3-dimensional Eddy Current Problems*, PhD thesis, University of Toronto, Canada, 1987.

[4] O. Michelsson, F. H. Uhlmann: *On the use of the 3D H-φ-Formulation for the forward solution for eddy current non-destructive testing*, IEEE Transactions on Magnetics, Vol. 34, no. 5, pp. 2672-2675, 1998.

[5] G. Kämmel, H. Franeck: *Einführung in die Methode der finiten Elemente*, Fachbuchverlag Leipzig, 1988.

[6] J. Shen, O. Sterz: *A mixed Calerkin and collocation approach for treating edge and corner problems in the boundary element method*, IEEE Transactions on Magnetics, Vol. 34, no. 5, pp. 3296-3299, 1998.

[7] J. Yuan, A. Kost: *A three-component boundary element algorithm for three-dimensional eddy current calculation*, IEEE Transactions on Magnetics, Vol. 30, no. 5, pp. 3028-3031, 1994.

[8] M. Guiggiani, A. Gigante: *A general algorithm for multidimensional Cauchy principal value integrals in the boundary element method*, Transactions of the ASME, Vol. 57, pp. 906-915, 1990.

[9] J. Berntsen, T. Espelid, A. Genz: *An adaptive multidimensional integration routine for a vector of integrals* ACM Trans. Math. Softw., vol. 17, no. 4, pp. 425-456, 1991.

[10] J. R. Bowler; S. A. Jenkins: *Eddy current probe impedance due to a volumetric flaw*, J. Applied Physics, 70(3): 1107-1114 (1990).

[11] A. Yaghjian: *Electric dyadic Green's function in the source region*, Proc. Of the IEEE, 68(2), 248-263, 1980.

[12] C. Emson: *Results for a hollow sphere in uniform field (benchmark problem 6)*, COMPEL, Vol. 7, no. 1, pp. 89-101, 1988.